Journal of Alloys and Compounds 516 (2012) 58–64

Contents lists available at SciVerse ScienceDirect

Journal of Alloys and Compounds

journal homepage: www.elsevier.com/locate/jallcom

Specific heat of rare earth cobaltates $RCoO_3$ (R = La, Pr and Nd)

Rasna Thakur[a,*], Archana Srivastava[b], Rajesh K. Thakur[a], N.K. Gaur[a]

[a] Department of Physics, Barkatullah University, Bhopal 462026, India
[b] Department of Physics, Sri Sathya Sai College for Women, Bhopal 462024, India

ARTICLE INFO

Article history:
Received 22 September 2011
Received in revised form
15 November 2011
Accepted 25 November 2011
Available online 6 December 2011

Keywords:
Specific heat
Thermal properties
Bulk modulus
Cobaltates

ABSTRACT

We have reported the temperature dependence (5 K ≤ T ≤ 1000 K) of the lattice contribution to the specific heat of rhombohedral $LaCoO_3$ and orthocobaltates $RCoO_3$ (R = Pr and Nd). The strong electron phonon interactions are present in these compounds and lattice distortions can affect them substantially. Thus Rigid Ion Model (RIM) is used for the first time to study the cohesive and thermal properties of the cobaltates $RCoO_3$ with rare earth cation (R = La, Pr and Nd). The values of specific heat calculated by us have shown remarkably good agreement with corresponding experimental data. In addition, the results on the temperature dependence of cohesive energy (ϕ), molecular force constant (f), Reststrahlen frequency (υ), Debye temperature (θ_D) and Gruneisen parameter (γ) are also reported.

1. Introduction

Recently, rare earth perovskite cobaltates of general formula $RCoO_3$ (R is a rare-earth element or Y) have attracted much interest due to not only the interesting physical properties [1,2] but also the technological applications [3–5] ranges over a wide variety of fields from sensor devices, gas separation membranes, chemical reactors catalyst to components in solid oxide fuel cells. All the $RCoO_3$ (R = rare-earth element or Y) systems with a 3D network of corner-sharing CoO_6 octahedra show an insulating ground state based on the diamagnetic low-spin state of trivalent cobalt that in the limit of fully localized electrons in strong crystal field corresponds to filled t_{2g} levels and empty e_g states (LS, $t_{2g}^6 e_g^0, S = 0$). With increasing temperature they undergo two magnetic transitions connected with excitations either to the intermediate spin state (IS, $t_{2g}^5 e_g^1$, $S = 1$,) or to the high spin state (HS, $t_{2g}^4 e_g^2$, $S = 2$,). The second magnetic transition is accompanied by an insulator–metal (I–M) transition. It has remained controversial whether this transition is from a LS to a HS state or to an IS state. Originally, the LS-HS scenario was proposed [6]. In this framework, the anomalies would be due to an increase of the thermal population of the HS state. However, it was later claimed that this interpretation is inconsistent with photoemission data [7]. Korotin et al. [8] performed a local-density approximation LDA + U calculation and pointed out that the IS state is energetically comparable to the LS state at zero temperature. The energy of the IS state crosses that of the LS state with increasing temperature in their calculation, corresponding to a LS-IS state transition. This LS-IS scenario is consistent with the results of a neutron diffraction measurement [9], magnetic susceptibility [9], photoemission spectroscopy [10], and X-ray absorption spectroscopy [10]. The spin transitions are further manifested by observable changes in the crystal structure since the ionic radius of Co^{3+} increases with increasing spin state (r_{LS} = 0.545 Å, r_{IS} = 0.560 Å and r_{HS} = 0.610 Å) and produces anomalies in thermal expansion [11–13]. Additionally, Co^{3+} ion in IS or HS state is expected to be Jahn–Teller active and some kind of CoO_6 octahedra distortion can be anticipated.

$LaCoO_3$ is a diamagnetic insulator at low temperatures with a low spin state (LS) of Co^{3+} (S = 0). The splitting energy of the ground state of the cobalt ions in the crystal electric field is comparable to the energy of the intra-atomic exchange interaction; hence, an increase in the temperature can bring about thermal excitation of electrons from the t_{2g} energy level to the e_g energy level. At $T \approx 100$ K, the Co^{3+} ions undergo a transition to the intermediate-spin state [9] and the system as a whole becomes paramagnetic. As the temperature increases to T = 500 K, there arises a high-spin paramagnetic state and the compound undergoes a semiconductor–metal transition [9]. With increasing the atomic number of rare-earth element, their ionic radius becomes smaller (Pr^{3+} and Nd^{3+}) due to the effect of Lanthanide Contraction. If we replace La with Praseodymium (Pr), the smaller ionic radius of Pr as compared to that of La provides a chemical pressure on the system which increases the crystal field splitting energy and stabilizes the LS state to higher temperatures. Thus, the infrared (IR) spectroscopy data [14] were interpreted on the assumption that the

* Corresponding author at: Superconductivity Research Lab, Department of Physics, Barkatullah University, Bhopal 462026, India. Tel.: +91 755 2491821; fax: +91 755 2491823.
E-mail address: rasnathakur@yahoo.com (R. Thakur).

0925-8388/$ – see front matter © 2011 Elsevier B.V. All rights reserved.
doi:10.1016/j.jallcom.2011.11.128

transition of Co ions from the LS to the IS state in $LaCoO_3$, $PrCoO_3$, and $NdCoO_3$ occurs at 120, 220, and 275 K, respectively. The data on the lattice thermal expansion, obtained for $LnCoO_3$ by X-ray powder diffraction [12], show that the transition temperatures increase with decreasing Ln radius. In particular, the characteristic temperatures of the transitions are ~70 and 540 K for $LaCoO_3$, ~260 and 600 K for $PrCoO_3$, and ~340 and 630 K for $NdCoO_3$. Recently, it has been claimed that Co^{3+} remains in the nonmagnetic LS state up to at least 300 K in $PrCoO_3$ [15] and up to 600 K in $RCoO_3$ with R = Nd, Sm, and Eu [16] based on NMR measurements by Itoh et al. [15,16]. For instance, another recent NMR study concluded that the transition takes place at 300 K in $NdCoO_3$ [17]. Moreover, Yan et al. [18] have also argued that a spin-state transition takes place in $PrCoO_3$ and $NdCoO_3$ at 200 and 300 K, respectively, based on magnetic susceptibility and thermal conductivity measurements. Hence, it is still controversial at what temperature Co^{3+} undergoes a spin-state transition, but at least it seems that it occurs at a temperature that is higher than that of $LaCoO_3$.

Most neutron diffraction or XRD experiments of $LaCoO_3$ have been interpreted in rhombohedral space group $R\bar{3}c$ [11,19] and no structural transitions are reported in the temperature interval 4.2–1248 K [20]. This rhombohedral symmetry involves an alternating rotation of the corner sharing CoO_6 octahedra along all three crystallographic axes of the undistorted, cubic perovskite parent structure. This symmetry allows only one Co–O distance and thus this space group is incompatible with cooperative Jahn–Teller (JT) distortion. Such distortion, while preserving the alternating rotation of the CoO_6 octahedra, lowers the symmetry to monoclinic subgroups of $R\bar{3}c$. Maris et al. [21] recently found the monoclinic distortion for $LaCoO_3$ by performing a high angular-resolution scan using synchrotron radiation, and they analyzed their XRD data based on $I2_1/a$ symmetry, which was well consistent with the observed JT distortion [21]. On the other hand space group of both $PrCoO_3$ and $NdCoO_3$ was reported to be orthorhombic Pnma [22].

Lots of experimental data on magnetic and structural properties of these materials are available but to the best of our knowledge, no systematic theoretical investigation of thermal and cohesive properties of these cobaltate were carried out in the past whereas it is well established that strong electron–phonon coupling is present in these compounds which governs the conduction mechanism in these cobaltate compounds. Hence the theoretical investigation of thermal properties of perovskite cobaltate seems to be important for the progress of this field; hence RIM is being employed for the first time to study the temperature dependence of cohesive energy (ϕ), molecular force constant (f), Reststrahlen frequency (υ), Debye temperature (θ_D) and Gruneisen parameter (γ) and specific heat of these rare earth cabaltate compounds. The essential of the RIM formalism and the results obtained from its application are presented in the subsequent sections.

2. Formalism of RIM

We have formulated the rigid ion model (RIM) [23] by incorporating the effects of the long-range (LR) Coulomb attraction, the short-range (SR) Hafemeister–Flygare (HF) [24] type overlap repulsion effective up to the second neighbour atoms. The formalism of RIM is derived from the following interatomic interaction potential [25–28] is given as:

$$\phi^R_{kk'}(r) = -\frac{e^2}{2}\sum_{kk'} Z_k Z_{k'} r^{-1}_{kk'} + \sum_i n_i b_i \beta_{kk'} \exp\left\{(r_k + r_{k'} - r_{kk'})/\rho_i\right\} + \frac{n'_i}{2} b_i \left[\beta_{kk} \exp\left\{(2r_k - r_{kk})/\rho_i\right\} + \beta_{k'k'} \exp\left\{(2r_{k'} - r_{k'k'})/\rho_i\right\}\right] \quad (1)$$

Here, first term is attractive LR coulomb interactions energy and the second term is overlap repulsive energy represented by the Hafemeister–Flygare-type (HF) interaction extended up to the second neighbour. Here, $r_{kk'}$ represents separation between the nearest neighbours while r_{kk} and $r_{k'k'}$ appearing in the next terms are the second neighbour separation. $r_k(r_{k'})$ is the ionic radii of k (k') ion. n (n') is the number of nearest (next nearest neighbour) ions. In ABO_3 (such as $LaCoO_3$, $PrCoO_3$ and $NdCoO_3$) perovskite structure, k represents cation (A, B) and k' denotes the (O_1, O_2) type of ions. The summation is performed over all the kk' ions. b_i and ρ_i are the hardness and range parameters for the ith cation–anion pair (i = 1, 2) respectively and $\beta_{kk'}$ is the Pauling coefficient [29] expressed as:

$$\beta_{kk'} = 1 + \left(\frac{Z_k}{N_k}\right) + \left(\frac{Z_{k'}}{N_{k'}}\right) \quad (2)$$

with Z_k ($Z_{k'}$) and N_k ($N_{k'}$) as the valence and number of electrons in the outermost orbit of k (k') ions respectively. The model parameters (hardness and range) are determined from the equilibrium condition:

$$\left[\frac{d\phi(r)}{dr}\right]_{r=r_0} = 0 \quad (3)$$

and the bulk modulus:

$$B = \frac{1}{9Kr_0}\left[\frac{d^2\phi(r)}{dr^2}\right]_{r=r_0} \quad (4)$$

Here, r_o and r are the interionic separations in the equilibrium and otherwise states of the system, respectively. The symbol K is the crystal structure constant. The model parameters (b_1, ρ_1 for the ion pair Co–O and b_2, ρ_2 for the ion pair La/Pr/Nd–O) obtained from the Eqs. (3) and (4) have been used to compute the thermal properties.

The lattice specific heat is calculated using the formula,

$$C_{\upsilon(\text{lattice})} = 9R\left(\frac{T}{\theta_D}\right)^3 \int_0^{\theta_D/T} \frac{e^x x^4}{e^x - 1} dx \quad (5)$$

And at very low temperature ($T < \theta_D/50$) the specific heat is calculated by using

$$C_{\upsilon(\text{lattice})} = \frac{12\pi^4}{5}\left[Nk_B\left[\frac{T}{\theta_D}\right]^3\right] p \quad (6)$$

here p is the number of atoms in one formula unit. N is the Avogadro number, k_B the Boltzmann constant, R is the universal gas constant and θ_D is Debye temperature. The Debye temperature (θ_D) is given by the expression,

$$\theta_D = \frac{h}{k_B}\left[\left(\frac{3nN}{4\pi}\right)\left(\frac{\rho}{M}\right)\right]^{1/2} V_m \quad (7)$$

where h is the plancks constant, n is the number of molecules in unit cell, ρ is the density of sample, M is the molecular weight and V_m is the average sound velocity.

$$\theta = \frac{h\upsilon}{k_B} \quad (8)$$

where υ is the reststrahlen frequency.

$$\upsilon = \frac{1}{2\pi}\left[\frac{f}{\mu}\right]^{1/2} \quad (9)$$

where μ is the reduced mass and f is the molecular force constant given by,

$$f = \frac{1}{3}\left[\phi''^{SR}_{kk'}(r) + \frac{2}{r}\phi'^{SR}_{kk'}(r)\right]_{r=r_0} \quad (10)$$

with $\phi^{SR}_{kk'}(r)$ as the short-range nearest neighbour part of $\phi(r)$ The primes over them denote the first and second-order derivatives

of the $\phi_{kk'}^{SR}(r)$ with respect to the interionic separation (r). The Gruneisen parameter is calculated using the relation,

$$\gamma = \frac{-r_0}{6}\left[\frac{\phi'''_{kk'}(r)}{\phi''_{kk'}(r)}\right]_{r=r_o} \quad (11)$$

where r_o is the equilibrium distance between the kth and k'th ions and the primes in $\phi_{kk'}(r)$ denoted the third-order and second-order derivatives of the $\phi_{kk'}(r)$ with respect to the inter-ionic separations (r). The results thus obtained are presented and discussed below.

3. Results and discussion

The values of input data like unit cell parameter (a, b, c) and interionic distances are taken from Refs. [11,30] for the evaluation of model parameters (b_1, ρ_1) and (b_2, ρ_2) corresponding to the ionic pairs Co^{3+}–O^{2-} and R^{3+}–O^{2-} (R = La^{3+}, Pr^{3+} and Nd^{3+}) at different temperatures ($5\,K \le T \le 1000\,K$) for $RCoO_3$. The values of model parameters (b_1, b_2, ρ_1 and ρ_2) at different temperature for various rare earth cobaltates are listed in Tables 1–6. The value of bulk modulus for the compounds under investigation is an important input parameter from the point of view of critical determination of model parameters, but a few available value of bulk modulus of $RCoO_3$ (R = La, Pr and Nd) shows large deviations, as reported by various investigators; e.g. the value of bulk modulus of $LaCoO_3$ was reported to be 122 GPa [31], 150 GPa [32] and 180 GPa [33] which makes the choice of bulk modulus as input parameter a difficult task. So we thought of making a study of the bulk modulus of the $RCoO_3$ (R = rare earth) on the basis of formulations of atoms in molecules theory (AIM) [34] which stated that the inverse of the bulk modulus is the simple weighted average of the atomic compressibilities [34]:

$$\kappa = \sum_i f_i \kappa_i \quad \text{and} \quad \frac{1}{B} = \sum_i f_i \frac{1}{B_i} \quad (12)$$

where $f_i = V_i/V$

where f_i is the fractional volume occupancy due to quantum subsystem i in a unit formula, B is the bulk modulus of the compound and k is its compressibility. The values of ionic radii of A-site cations, are taken from [35] and the data on atomic compressibility from [36]. The values obtained by us are reported as B_0 in Tables 1, 3 and 5. In R$\bar{3}$c symmetry of $LaCoO_3$, all of the Co–O bond lengths are identical [11], so JT distortion cannot exist. However, unlike space group R$\bar{3}$c, there are unequal Co–O bond lengths in space group $I2_1/a$ [21], indicating that this compound is JT-distorted. If we investigate the rare earth cobaltates $RCoO_3$ (R = La, Pr and Nd) where the R-site cation radius reduces down the series, the buckling of the Co–O–Co angle progressively increases, which leads to increased distortions of the lattice. As the cation radius decreases down the series, the tolerance factor ($t = (r_R + r_O)/\sqrt{2}(r_{Co} + r_O)$) where r_R is the ionic radius of R (R = La, Pr and Nd), r_{Co} is the ionic radius of cobalt and r_O is the ionic radius of oxygen, whose value for $LaCoO_3$ cubic perovskite structure is around 1, also reduces to orthorhombic form 0.9377 for $PrCoO_3$ and 0.9319 for $NdCoO_3$ and a decrease in the unit cell volume can be observed. This decrease in cell volume corresponds to increase in bulk modulus of the compound. This is evident from our results depicted in Tables 1–6 and in Figs. 1–3; the bulk modulus of $NdCoO_3$ is greater than that of $PrCoO_3$ and $PrCoO_3$ is greater than that of $LaCoO_3$. At the same time, the debye temperature is expected to increase as well down the series from $LaCoO_3$ to $NdCoO_3$. An increase in temperature corresponds to increase in bulk modulus (B_0) of $RCoO_3$ (R = Pr and Nd) and the same can be observed from Figs. 1–3. The bulk modulus follows a quasi linear increase in the value as the temperature increases from $100\,K \le T \le 1000\,K$. We considered the effect of charge, size mismatch between A and B site cation in various LS, IS and HS states of compounds on the bulk modulus of the compounds. The formal expressions for calculation of the Jahn–Teller (JT) distortions, cation size, charge mismatch and the bulk modulus of the distorted perovskite cobaltates are same

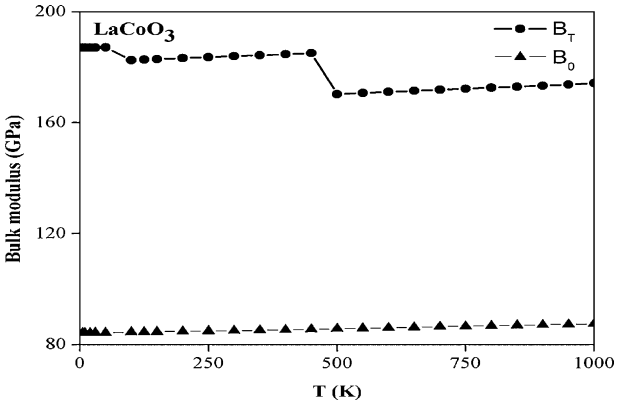

Fig. 1. Variation of bulk modulus (B_o and B_T) of rhombohedral $LaCoO_3$ as a function of temperature where the solid line (—) with solid triangle (▲) and the solid line (—) with solid circle (●) represent B_0 and B_T, respectively.

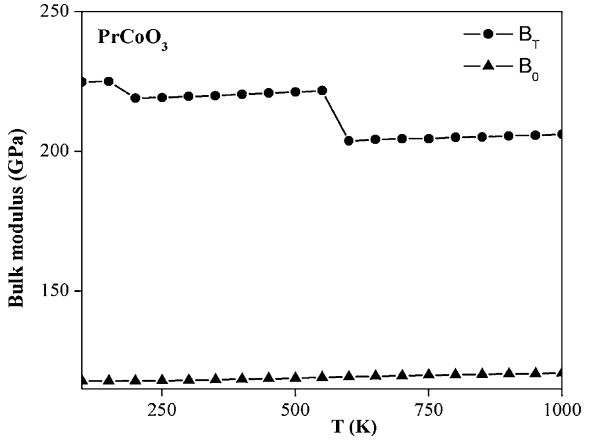

Fig. 2. Variation of bulk modulus (B_o and B_T) of orthorhombic $PrCoO_3$ as a function of temperature where the solid line (—) with solid triangle (▲) and the solid line (—) with solid circle (●) represent B_0 and B_T, respectively.

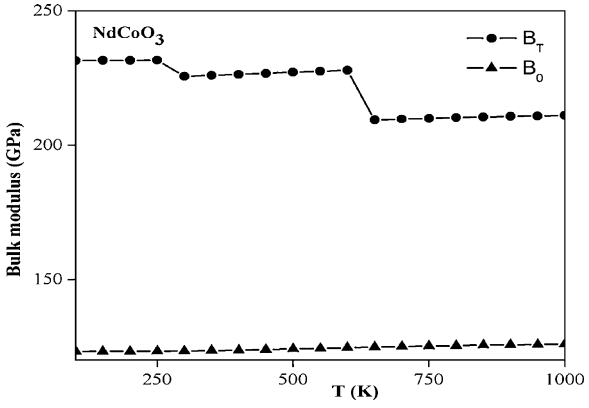

Fig. 3. Variation of bulk modulus (B_o and B_T) of orthorhombic $NdCoO_3$ as a function of temperature where the solid line (—) with solid triangle (▲) and the solid line (—) with solid circle (●) represent B_0 and B_T, respectively.

Table 1
The model parameters, bulk modulus (based on AIM theory), cohesive and thermal properties of rhombohedral $LaCoO_3$ at low temperature (≤110 K), intermediate temperature (≥150 K) and high temperature (≥500 K).

T (K)	Model parameters				Properties					
	$b_1 \times 10^{-19}$ (J) (Co–O)	$b_2 \times 10^{-19}$ (J) (La–O)	ρ_1 (Å) (Co–O)	ρ_2 (Å) (La–O)	B_0 (GPa) (AIM)	Φ (eV)	f (N/m)	υ (THz)	θ_D (K)	γ
<110	3.157	1.814	0.385	0.654	84.2	−134.12	16.28	6.39	307.31	1.92
>150	3.079	1.811	0.378	0.646	85.03 122.0[a]	−134.06	16.55	6.45	309.81	1.95
>500	2.797	1.819	0.361	0.623	87.49	−133.83	17.35	6.6	317.28	2.07 (2–3)[b]

[a] Ref. [31].
[b] Ref. [11].

Table 2
The model parameters, bulk modulus (distorted perovskite), cohesive and thermal properties of rhombohedral $LaCoO_3$ at low temperature (≤110 K), intermediate temperature (≥150 K) and high temperature (≥500 K).

T (K)	Model parameters				Properties					
	$b_1 \times 10^{-19}$ (J) (Co–O)	$b_2 \times 10^{-19}$ (J) (La–O)	ρ_1 (Å) (Co–O)	ρ_2 (Å) (La–O)	B_T (GPa)	Φ (eV)	f (N/m)	υ (THz)	θ_D (K)	γ
<110	1.365	2.176	0.221	0.4	187.02	−149.45	36.16	9.53	457.99 480[a]	3.11
>150	1.654	1.128	0.222	0.401	183.97 180[b]	−148.72	35.8	9.49	455.72	3.13
>500	1.584	1.221	0.223	0.403	174.24	−146.5 −144.54[c]	34.56	9.32	447.74	3.16

[a] Ref. [38].
[b] Ref. [33].
[c] Ref. [37].

Table 3
The model parameters, bulk modulus (based on AIM theory), cohesive and thermal properties of orthorhombic $PrCoO_3$ at low temperature (≤110 K), intermediate temperature (≥150 K) and high temperature (≥500 K).

T (K)	Model parameters				Properties					
	$b_1 \times 10^{-19}$ (J) (Co–O)	$b_2 \times 10^{-19}$ (J) (Pr–O)	ρ_1 (Å) (Co–O)	ρ_2 (Å) (Pr–O)	B_0 (GPa) (AIM)	Φ (eV)	f (N/m)	υ (THz)	θ_D (K)	γ
<110	2.52	2.03	0.319	0.495	117.82	−142.05 −144.54[a]	23.13	7.6	365.19	2.33 (2–3)[b]
>150	2.44	1.99	0.317	0.491	118.1	−142	23.26	7.62	366.2	2.35
>500	2.25	1.86	0.303	0.459	120.64	−141.47	24.37	7.8	374.85	2.49

[a] Ref. [37].
[b] Ref. [11].

Table 4
The model parameters, bulk modulus (distorted perovskite), cohesive and thermal properties of orthorhombic $PrCoO_3$ at low temperature (≤110 K), intermediate temperature (≥150 K) and high temperature (≥500 K).

T (K)	Model parameters				Properties					
	$b_1 \times 10^{-19}$ (J) (Co–O)	$b_2 \times 10^{-19}$ (J) (Pr–O)	ρ_1 (Å) (Co–O)	ρ_2 (Å) (Pr–O)	B_T (GPa)	Φ (GPa)	f (N/m)	υ (THz)	θ_D (K)	γ
<110	1.4	1.21	0.198	0.318	225.01	−153.52	44.19	10.51	504.74	3.51
>150	1.38	1.23	0.201	0.322	219.66	−153.01	43.27	10.38	499.45	3.47
>500	1.37	1.22	0.203	0.316	206.09	−150.59	41.64	10.2	489.93	3.5

Table 5
The model parameters, bulk modulus (based on AIM theory), cohesive and thermal properties of orthorhombic $NdCoO_3$ at low temperature (≤110 K), intermediate temperature (≥150 K) and high temperature (≥500 K).

T (K)	Model parameters				Properties					
	$b_1 \times 10^{-19}$ (J) (Co–O)	$b_2 \times 10^{-19}$ (J) (Nd–O)	ρ_1 (Å) (Co–O)	ρ_2 (Å) (Nd–O)	B_0 (GPa) (AIM)	Φ (eV)	f (N/m)	υ (THz)	θ_D (K)	γ
<110	2.44	2.06	0.312	0.485	123.23	−143.06 −144.54[a]	24.08	7.72	370.69	2.38 (2–3)[b]
>150	2.4	2	0.305	0.471	124.37	−142.8	24.58	7.8	374.56	2.44
>500	2.37	1.91	0.297	0.45	126	−142.4	25.32	7.91	380.15	2.54

[a] Ref. [37].
[b] Ref. [11].

Table 6
The model parameters, bulk modulus (distorted perovskite), cohesive and thermal properties of orthorhombic $NdCoO_3$ at low temperature (≤110 K), intermediate temperature (≥150 K) and high temperature (≥500 K).

T (K)	Model parameters				Properties					
	$b_1 \times 10^{-19}$ (J) (Co–O)	$b_2 \times 10^{-19}$ (J) (Nd–O)	ρ_1 (Å) (Co–O)	ρ_2 (Å) (Nd–O)	B_T (GPa)	Φ (eV)	f (N/m)	υ (TH_z)	θ_D (K)	γ
<110	1.36	1.27	0.195	0.315	231.44 230[a]	−154.17	45.22	10.57	508.01	3.54
>150	1.34	1.29	0.198	0.319	225.61	−153.23	44.16	10.45	502.05	3.49
>500	1.36	1.28	0.202	0.314	211.1	−151.13	42.42	10.24	492.04	3.53

[a] Ref. [31].

as defined earlier [28]. The expression for the bulk modulus of the distorted perovskite cobaltate is:

$$B_T = \frac{K_S B_0 \sigma_m \cos\omega}{\exp(\Delta_{JT})\sigma_C} \quad (13)$$

where K_S is the spin order-dependent constant of proportionality, and its value is less than 1 for the ferromagnetic state and more than 1 for paramagnetic state, B_0 is the bulk modulus for undistorted structure calculated on the basis of AIM theory, σ_m is the size mismatch, σ_c is the charge mismatch, Δ_{JT} is JT distortion of CoO_6 octahedra and $\cos\omega$ is the effect of buckling of the Co–O–Co angle. An increase in temperature corresponds to increase in bulk modulus (B_T) of $RCoO_3$ (R = La, Pr and Nd) but sudden decrease at $T \sim 100$ and 500 K for $LaCoO_3$ (Fig. 1), ~200 and 600 K for $PrCoO_3$ (Fig. 2) and ~300 and 650 K for $NdCoO_3$ (Fig. 3) is due to the excitation of Co ions to IS and HS as determined by Asai et al. [9] and Yan et al. [18]. The value of bulk modulus of the distorted structure is presented in Tables 2, 4 and 6 as B_T. It can be observed from the Tables 2, 4 and 6 that distortions change the bulk modulus B_0 and the calculated value after considering the effect of various distortions is seemingly high compared to B_0 for $RCoO_3$ with rare earth cation (R = La, Pr and Nd) at R site. The bulk modulus calculated on the basis of AIM theory is found to be in satisfactory agreement with the experimental value. The calculated value of bulk modulus 183.97 GPa and 231.44 GPa for $LaCoO_3$ and $NdCoO_3$ are close to the reported value of 180 GPa [31] for $LaCoO_3$ and 230 GPa for $NdCoO_3$ by Zhou et al. [33].

As cohesive energy is the measure of strength of the force binding the atoms together in solids. We have applied RIM to compute the cohesive energy and thermal properties of $RCoO_3$ (R = La, Pr and Nd) compounds and reported them in Tables 1–6. Cohesive energy is calculated by using Eq. (1). Our calculated values of cohesive energy −146.50 eV, −142.05 eV and −143.06 eV for $LaCoO_3$ and $PrCoO_3$ and $NdCoO_3$ seems to be realistic as they are near to the reported value −144.54 eV for the compound $SmCoO_3$ [37] at room temperature, which is a member of the cobaltate family. The negative value of cohesive energy indicates the stability of the compound. The frequency of vibration of positive ion lattice with respect to negative ion lattice obtained from this model is reported here as the Reststrahlen frequency (υ). Since the Restrahalen frequency is directly proportional to the molecular force constant (f) therefore both of them vary with the temperature accordingly for these compounds. A precise experimental analysis of reststrahlen frequency is needed to verify the results of present calculations. The Debye tempertature has played an important role to understand the thermophysical properties of materials. It is basically a measure of the vibrational response of the material and therefore, intimately connected with properties like the specific heat, thermal expansion and vibrational entropy. Therefore, we have computed the Debye temperatures at 5 K ≤ T ≤ 1000 K. The higher value of Debye temperature indicates the higher phonon frequency of the compounds. Our calculated value of 457.99 K (upto 10 K) for $LaCoO_3$ is comparable to the reported value of 480 K obtained by He et al. experimentally [38]. The calculated value of Gruneisen parameter seems to be correct since its value lies between 2 and 3 (Tables 1, 3 and 5) as obtained for perovskite structure materials [11]. From Tables 2, 4 and 6 it can be seen that its value is above 3 which indicated the enhanced anharmonic effect in the higher temperature regime. Besides, we have studied the temperature evolution of the lattice specific heat of $LaCoO_3$ and $RCoO_3$ (R = Pr and Nd) for the various temperature range 100 K ≤ T ≤ 1000 K. The calculated specific heat values of $LaCoO_3$ in the temperature range 0 to 80 K are displayed in Fig. 4. Here the specific heat revealed by using interionic potential is in good agreement with the available experimental data of Kyomen et al. [39].

The specific heat values calculated by us for $LaCoO_3$ at temperature (100 K ≤ T ≤ 1000 K) are displayed in the main panel of Fig. 5 and found to be in good agreement with the measured data [40] for temperature upto 400 K. Our results have followed a trend more or less similar to those exhibited by the experimental curve. A sharp peak is observed in the measured specific heat curve around 500 K due to insulator to metal transition. The anomalies between the present and experimental specific heat at $T \sim 500$ K (Fig. 5) might be due to the exclusion of magnetic contribution in our interaction potential. The calculated specific heat of $LaCoO_3$ at very low temperature region $T < (\theta_D/50)$ are estimated with the help of Eq. (6) are shown in the inset of Fig. 5. It is found that it follows the similar trend as shown experimentally [38]. The calculated lattice specific heat (solid line with solid circle) gives debye temperature (457.99 K) which is consistent with debye temperature (480 K) (Ref. [38]). The discrepancy in the present and estimated values [38] of Debye temperature might be due the non inclusion of electronic contribution in our interaction potential. The specific heat calculated for $RCoO_3$ (R = Pr and Nd) at temperature 100 K ≤ T ≤ 1000 K are displayed in Figs. 6 and 7 and found to be in good agreement

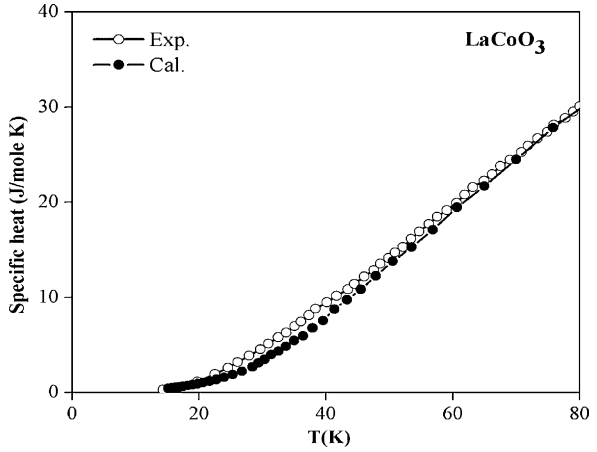

Fig. 4. Variation of calculated specific heat of $LaCoO_3$ as a function of temperature (0 ≤ T ≤ 80 K). The solid line with dark circle (–●–) and solid line with open circle (–○–) represent the model calculation and experimental curve of Kyomen et al. [39].

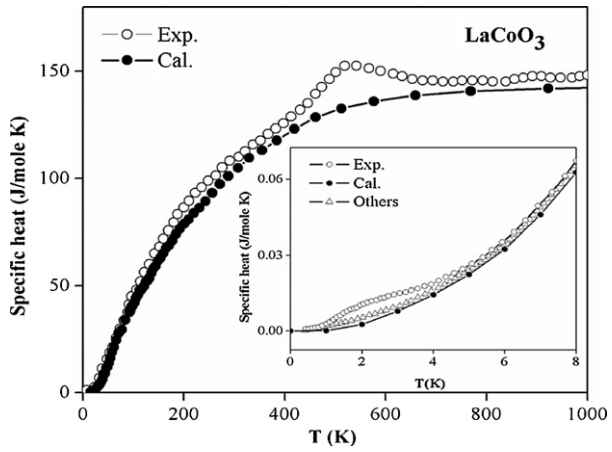

Fig. 5. Variation of calculated specific heat $LaCoO_3$ as a function of temperature ($0 \le T \le 1000$ K). The solid line with dark circle (–●–) and solid line with open circle (–○–) represent the model calculation and experimental values of Stolen et al. [40] (main panel). The inset shows temperature dependence of the calculated specific heat at very low temperature ($0 \le T \le 8$ K) by solid line with solid circle (–●–) and its comparison with experimental curve of He et al. [38].

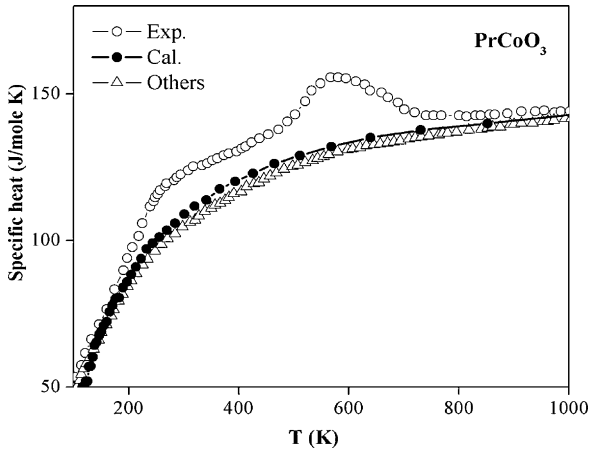

Fig. 6. Variation of calculated specific heat of $PrCoO_3$ as a function of temperature ($100\text{ K} \le T \le 1000$ K). The solid line with dark circle (–●–), solid line with open circle (–○–) and solid line with open triangle (–△–) represent the present calculation, experimental curve of Knizek et al. [30] and calculated curve of Knizek et al. [30] respectively.

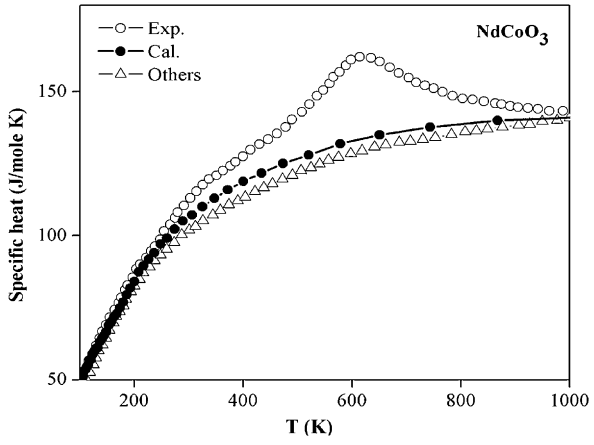

Fig. 7. Variation of calculated specific heat of $NdCoO_3$ as a function of temperature ($100\text{ K} \le T \le 1000$ K). The solid line with solid circle (–●–) and the solid line with open circle (–○–) and solid line with open triangle (–△–) represent the present calculation, experimental curve of Knizek et al. [30] and calculated curve of Knizek et al. [30] respectively.

with the measured value obtained by Knizek et al. [29]. Our results have followed a trend more or less similar to those exhibited by the experimental curve. The calculated specific heat for $RCoO_3$ (R = Pr and Nd) for temperature range upto 300 K follows the similar trend as shown experimentally [30]. A sharp peak is observed in the experimental specific heat curve at 260 K and 600 K for $PrCoO_3$ and 340 K and 630 K for $NdCoO_3$ are due to the transition from magnetic state and insulator metal transition (I–M). This feature is not obtained in our calculated results and this might be due to the exclusion of the $C_{Co,spin}$ and $C_{electronic}$. The former term is associated with local transitions in cobalt ions while the latter term anticipates an existence of bandlike charge carriers contribution at high temperatures only where $RCoO_3$ systems transform to a metallic state. It is noted that slight deviation of calculated specific heat from the estimated values (solid line with open triangle) might be due to $C_{dilatation}$ (see Figs. 6 and 7), which reflects both the harmonic and anharmonic effects associated with lattice dilation and crystal-field splitting of the rare-earth electronic ground state ($C_{Ln,CF}$).

4. Conclusion

A detailed cohesive and thermal properties of rare earth cobaltates $RCoO_3$ (R = La, Pr and Nd) at temperature $5\text{ K} \le T \le 1000$ K has been presented in this paper. It is interesting to note from earlier discussion that the agreement between experimental and our theoretical results on specific heat is reasonably good. The specific heat curves (Figs. 5, 6 and 7) show a sharp peaks at 500 K for $LaCoO_3$, 260 K and 600 K for $PrCoO_3$ and 340 K and 630 K for $NdCoO_3$. In our results sharp peaks could not be observed in specific heat curve on $RCoO_3$ (R = La, Pr and Nd) due to the exclusion of electronic and magnetic contribution in the present potential. As the dominant contribution to the specific heat is the phonon term which shows that these compounds are Debye-type solid. RIM is successful in predicting lattice contribution of the specific heat. On inspection of Figs. 1–3 there is sudden decrease in bulk modulus at $T \sim 100$ and 500 K for $LaCoO_3$ (Fig. 1), ~200 and 600 K for $PrCoO_3$ (Fig. 2) and ~300 and 650 K for $NdCoO_3$ (Fig. 3). This might be due to the excitation of Co ions to intermediate spin (IS) and high spin (HS) and are similar to those reported by Asai et al. [9] and Yan. et al. [18]. Here, some of the results on cohesive and thermal properties could not be compared due to lack of experimental data on them. These results are at present of academic interest but they will certainly work as a guide to the experimental workers in future.

A successful description of cohesive and thermal properties achieved for such complicated system $RCoO_3$ (R = La, Pr and Nd) can be considered remarkable in view of the inherent simplicity of RIM and its less parametric nature. The beauty of present model is that it has predicted the cohesive properties of cobaltates with the same success as their thermal properties. The results of the present investigation can be further improved by the incorporating the effects of electronic and magnetic contribution in the present potential.

Acknowledgements

The authors are thankful to the University Grant Commission (UGC), New Delhi for providing the financial support.

References

[1] Z. Ropka, R. Radwanski, Phys. Rev. B 67 (2003) 172401.
[2] Y. Kobayashi, T. Nakajima, K. Asai, J. Magn. Magn. Mater. 83 (2004) 272.
[3] J.S. Park, K.K. Yu, H.K. Lee, H.R. Bae, Y.P. Lee, V.G. Prokhorv, J. Korean Phys. Soc. 46 (2005) S201.
[4] H. Chang, C.L. Chen, T. Garrett, X.H. Chen, X.D. Xiang, C.W. Chu, Q.Y. Zhang, C. Dong, Appl. Phys. Lett. 80 (2002) 4333.
[5] V.G. Prohkorov, Y.P. Lee, K.W. Kim, V.M. Ishchuk, I.N. Chukanova, Appl. Phys. Lett. 80 (2002) 2352.
[6] J.B. Goodenough, J. Phys. Chem. Solids 6 (1958) 287.

[7] M. Abbate, J.C. Fuggle, A. Fujimori, L.H. Tjeng, C.T. Chen, R. Potze, G.A. Sawatzky, H. Eisaki, D. Uchida, Phys. Rev. B 47 (1993) 16124.
[8] M.A. Korotin, S. Yu Ezhov, I.V. Solovyev, V.I. Anisimov, D.I. Khomskii, G.A. Sawatzky, Phys. Rev. B 54 (1996) 5309.
[9] K. Asai, A. Yoneda, O. Yokokura, J.M. Tranquada, G. Shirane, K. Kohn, J. Phys. Soc. Jpn. 67 (1998) 290.
[10] T. Saitoh, T. Mizokawa, A. Fujimori, M. Abbate, Y. Takeda, M. Takano, Phys. Rev. B 55 (1997) 4257.
[11] P.G. Radaelli, S.W. Cheong, Phys. Rev. B 66 (2002) 094408.
[12] K. Knizek, Z. Jirak, J. Hejtmanek, M. Veverka, M. Marysko, G. Maris, T.T.M. Palstra, Eur. Phys. J. B 47 (2005) 213.
[13] K. Berggold, M. Kriener, P. Becker, M. Benomar, M. Reuther, C. Zobel, T. Lorenz, Phys. Rev. B 78 (2008) 134402.
[14] L. Sudheendra, M.M. Seikh, A.R. Raju, C. Narayana, Chem. Phys. Lett. 340 (2001) 275.
[15] M. Itoh, M. Mori, S. Yamaguchi, Y. Tokura, Physica B 902 (1999) 259–261.
[16] M. Itoh, J. Hashimoto, S. Yamaguchi, Y. Tokura, Physica B 510 (2000) 281–282.
[17] A. Ghoshray, B. Bandyopadhyay, K. Ghoshray, V. Morchshakov, K. Barner, I.O. Troyanchuk, H. Nakamura, T. Kohara, G.Y. Liu, G.H. Rao, Phys. Rev. B 69 (2004) 064424.
[18] J.Q. Yan, J.S. Zhou, J.B. Goodenough, Phys. Rev. B 69 (2004) 134409.
[19] G. Thornton, B.C. Tofield, A.W. Hewat, J.Solid State Chem. 61 (1986) 301.
[20] Y. Kobayashi, T. Mitsunaga, G. Fujinawa, T. Arii, M. Suetake, K. Asai, J. Harada, J. Phys. Soc. Jpn. 69 (2000) 3468.
[21] G. Maris, Y. Ren, V. Volotchaev, C. Zobel, T. Lorenz, T.T.M. Palstra, Phys. Rev. B 67 (2003) 224423.
[22] H.W. Brinks, H. Fjellvag, A. Kjekshus, B.C. Hauback, J. Solid State Chem. 147 (1999) 464.
[23] N.K. Gaur, R. Choithrani, A. Srivastava, Solid State Commun. 145 (2008) 308–311.
[24] D.W. Hafemiester, W.H. Flygare, J. Chem. Phys. 43 (1965) 795.
[25] N. Kaur, R. Mohan, N.K. Gaur, R.K. Singh, J. Alloys Compd. 509 (2011) 6077–6082.
[26] N. Kaur, R. Mohan, N.K. Gaur, R.K. Singh, J. Alloys Compd. 491 (2010) 284.
[27] R. Choithrania, N.K. Gaur, R.K. Singh, J. Alloys Compd. 480 (2009) 727.
[28] A. Srivastava, N.K. Gaur, J. Magn. Magn. Mater. 321 (2009) 3854–3865; A. Srivastava, N.K. Gaur, J. Phys.: Condens. Matter 21 (2009) 096001.
[29] L. Pauling, Z. Kristallogr. 67 (1928) 377.
[30] K. Knizek, J. Hejtmanek, Z. Jirak, P. Tomes, P. Henry, G. Andre, Phys. Rev. B 79 (2009) 134103.
[31] J.S. Zhou, J.Q. Yan, J.B. Goodenough, Phys. Rev. B 71 (2005) 220103.
[32] T. Vogt, J.A. Hriljac, N.C. Hyatt, P. Woodward, Phys. Rev. B 67 (2003) 140401.
[33] A.L. Cornelius, S. Kletz, J.S. Schilling, Physica C 197 (1992) 209.
[34] A.M. Pendas, A. Costales, M.A. Blanco, J.M. Recio, V. Luana, Phys. Rev. B 62 (2000) 13970–13978.
[35] R.D. Shannon, Acta Crystallogr. A 32 (1976) 751.
[36] C. Kittel, Introduction to Solid State Physics 5th edn (New York: Wiley) www.webelements.com.
[37] M.A. Farhan, M.J. Akhtar, J. Phys.: Condens. Matter 22 (2010) 075402.
[38] C. He, H. Zheng, J.F. Mitchell, M.L. Foo, R.J. Cava, C. Leighton, Appl. Phys. Lett. 94 (2009) 102514.
[39] T. Kyomen, Y. Asaka, M. Itoh, Phys. Rev. B 71 (2005) 024418.
[40] S. Stolen, F. Gronvold, H. Brinks, T. Atake, H. Mori, Phys. Rev. B 55 (1997) 14103.